PHYSICAL REVIEW C **96**, 011302(R) (2017)

Recoil distance method lifetime measurement of the 2_1^+ state in ^{94}Sr and implications for the structure of neutron-rich Sr isotopes

A. Chester,[1,*] G. C. Ball,[2] R. Caballero-Folch,[2] D. S. Cross,[1] S. Cruz,[2,3] T. Domingo,[1] T. E. Drake,[4] A. B. Garnsworthy,[2] G. Hackman,[2] S. Hallam,[2] J. Henderson,[2] R. Henderson,[2] W. Korten,[5] R. Krücken,[2,3] M. Moukaddam,[2] B. Olaizola,[6] P. Ruotsalainen,[2] J. Smallcombe,[2] K. Starosta,[1,†] C. E. Svensson,[6] J. Williams,[1] and K. Wimmer[7]

[1]*Department of Chemistry, Simon Fraser University, 8888 University Drive, Burnaby, British Columbia, Canada V5A 1S6*

[2]*TRIUMF, 4004 Wesbrook Mall, Vancouver, British Columbia, Canada V6T 2A3*

[3]*Department of Physics and Astronomy, University of British Columbia, 6224 Agricultural Road, Vancouver, British Columbia, Canada V6T 1Z1*

[4]*Department of Physics, University of Toronto, Toronto, Ontario, Canada M5S 1A7*

[5]*Irfu, CEA, Université Paris-Saclay, F91191 Gif-sur-Yvette, France*

[6]*Department of Physics, University of Guelph, 50 Stone Road East, Guelph, Ontario, Canada N1G 2W1*

[7]*Department of Physics, University of Tokyo, 7 Chome-3-1 Hongo, Bunkyo, Tokyo 113-8654, Japan*

(Received 19 December 2016; revised manuscript received 13 February 2017; published 6 July 2017)

A high precision lifetime measurement of the 2_1^+ state in ^{94}Sr was performed at TRIUMF's ISAC-II facility by coupling the recoil distance method implemented via the TIGRESS integrated plunger with unsafe Coulomb excitation in inverse kinematics. Due to limited statistics imposed by the use of a radioactive ^{94}Sr beam, a likelihood ratio χ^2 method was derived and used to compare experimental data to Geant4 simulations. The $B(E2; 2_1^+ \rightarrow 0_1^+)$ value extracted from the lifetime measurement of $7.80^{+0.50}_{-0.40}$(stat.) $\pm$ 0.07(sys.) ps is approximately 25% larger than previously reported while the relative error has been reduced by a factor of approximately 8. A baseline deformation has been established for Sr isotopes with $N \leqslant 58$ which is a necessary condition for the quantum phase transition interpretation of the onset of deformation in this region. A comparison to existing theoretical models is presented.

DOI: 10.1103/PhysRevC.96.011302

I. Introduction. The neutron-rich Sr and Zr isotopes are characterized by a sudden onset of quadrupole deformation at neutron number $N = 60$. In the Zr isotopes, this phenomenon has been described as type-II shell evolution, driven through the central and tensor components of the effective interaction [1]. The occupation of the proton $0g_{9/2}$ orbital lowers the neutron $0g_{7/2}$ and $0h_{11/2}$ orbitals as described in recent Monte Carlo shell model calculations [2]. Consequently, the excitation of protons into the $0g_{9/2}$ involves a significant rearrangement of nucleons. The near-spherical ground state and prolate excited state configurations do not mix and the rapid onset of deformation observed in the Zr isotopes occurs when the prolate configuration becomes the ground state at $N = 60$ ^{100}Zr [2]. This abrupt change in ground state shape as a function of neutron number N has been identified as an example of a quantum phase transition (QPT) from a spherical phase to a deformed phase [2]. A spherical ground state band and deformed excited state band built on the 0_2^+ state, consistent with the QPT picture, was recently observed in ^{96}Zr [3]. It should be noted that this QPT-based shell evolution mechanism requires the existence of a unique-parity orbital (e.g., the $0g_{9/2}$) above a closed shell; the only known cases which meet this criterion are the Zr and Sr isotopes [2].

Though the emphasis is usually put on the phase transition behavior at $N = 60$, it is equally surprising that there is no enhancement of collectivity when adding up to eight neutrons beyond the $N = 50$ shell closure, which points to the robustness of both the $Z = 38$ and $Z = 40$ proton subshell closures in the Sr and Zr isotopes. This delay of the onset of collectivity was first observed for the Sr isotopes following the measurement of extremely low $B(E2; 2_1^+ \rightarrow 0_1^+)$ values of approximately $0.020e^2b^2$ from ^{90}Sr to ^{96}Sr [4] which are an order of magnitude less than those observed for ^{98,100}Sr [5–7]. These values are more than a factor of 2 lower than what would be expected from Grodzin's rule [8,9] based on the nearly constant energies of the 2_1^+ states between 815 and 837 keV in these isotopes. In fact, the Sr and neighboring Zr isotopes form a group of the least collective nuclei beyond ^{56}Ni, similar only to the Sn and Te isotopes around ^{132}Sn and some neutron-deficient Pb isotopes [10].

While no detailed shell model calculations similar to those found in Ref. [2] are available for exploring the potential QPT behavior in the Sr isotopes, the limited experimental data in this region—including energies and transition rates [10,11]—show many similarities to the Zr isotopes which have been described using the QPT framework. Existing theoretical calculations for the Sr isotopes have been performed using a variety of approaches, including the quadrupole plus pairing Hamiltonian (QPH) [12], the Nilsson-Strutinsky method with the Woods-Saxon potential (N-S WS) [13], relativistic mean field calculations (RMF) [14], finite range liquid drop model (FRDM) [15], and approximations to the Strutinsky energy theorem (ETFSI) [15]. While these approaches reproduce the onset of deformation in Sr qualitatively, they differ on the details of the deformation parameters. Similar to the Zr isotopes, in the transitional region around $N = 60$ different

*ascheste@sfu.ca
†starosta@sfu.ca

shapes are expected to coexist in a narrow energy range as recently confirmed for ^{96,98}Sr [16]. The approximately constant and nearly spherical ground state shapes in the nearby Sr nuclei with $N < 60$ are a necessary (but not sufficient) condition for the applicability of the QPT interpretation defined by the transition from a spherical to deformed phase. Based on the preceding arguments, a high-precision lifetime measurement of the 2_1^+ state in ^{94}Sr has been performed to elucidate whether the onset of collectivity is as sudden as generally assumed. The development of radioactive ion beams at facilities such as TRIUMF, Canada's National Laboratory for Particle and Nuclear Physics, has in turn driven the development of experimental techniques and the construction of new equipment which can take advantage of the many opportunities such beams provide. In order to perform this measurement, a new device for recoil distance method (RDM) lifetime measurements, the TIGRESS Integrated Plunger (TIP) was constructed and employed.

II. Experimental details. An RDM experiment was performed to measure the lifetime of the 2_1^+ state in ^{94}Sr populated by Coulomb excitation (Coulex). A detailed and comprehensive review of the principles of RDM measurements is given in Ref. [17]. Coupling RDM lifetime measurements and Coulex reactions has many advantages, two of which are highlighted here. First, the method utilizes the large Coulex cross section to enable high-precision lifetime measurements with low-intensity radioactive beams and is not, in general, sensitive to beam contamination or fluctuations in beam intensity. Second, since the Coulex reaction is being used only as a tool to populate excited states, Coulex-RDM experiments can be run near or above the Coulomb barrier, thus enhancing the reaction cross section, because interference from the nuclear force on the excitation process does not negatively impact the measurement. Further, Coulex-RDM does not require any knowledge of the absolute reaction cross section or absolute efficiency of the detection systems used for the measurement. For these reasons, this method is an attractive approach for performing experiments at radioactive ion beam facilities where pure beams of constant and/or high intensity are not always available. Lifetime measurements have been recognized as a complementary technique to traditional Coulex experiments for investigating the structure of low-lying excited states, particularly for understanding the mechanisms of shape coexistence in the $A \approx 100$, $N \approx 60$ region [18]. To the best knowledge of the authors, this is the first application of Coulex-RDM in inverse kinematics to low-energy radioactive beams, which has been highlighted as a method of special importance [17].

In the presented experiment, a beam of radioactive ^{94}Sr with a fluctuating intensity of $2–5\times10^4$ particles per second was provided by the ISAC facility at TRIUMF and accelerated to 2.979 MeV/A (280 MeV) using the ISAC-II linear accelerator [19]. Accelerated ^{94}Sr was delivered to the TIP plunger mounted at the center of the TIGRESS array [20] and Coulomb excited to the 2_1^+ state on a movable 1.09 mg/cm^2 Al target in inverse kinematics. Excited ^{94}Sr nuclei emerged from the target and decayed in flight to the 0_1^+ ground state by the emission of a γ-ray with rest energy $E_0 = 836.9$ keV after traversing a distance governed by their speed and the lifetime of the 2_1^+ excited state. A stationary 3.69 mg/cm^2 Cu degrader, fixed at the center position of the TIP scattering chamber downstream from the target, further slowed the ^{94}Sr nuclei. The fixed degrader position ensures that the solid angle coverage of all detectors downstream from the degrader is consistent throughout the course of the measurement. Doppler-shifted γ rays emitted in flight between the target and degrader have a different energy distribution than those emitted after the degrader due to the change in velocity. The ratio of γ rays emitted after the degrader (the "slow component") to those emitted in flight between the target and degrader (the "fast component") changes as a function of target-degrader separation distance and the lifetime of the transition can be inferred from the change in the intensity ratio of the fast and slow components as the distance between the target and degrader is varied.

Recoil distance method lifetime measurements using TIP can be significantly enhanced by coupling the plunger to one of the ancillary detection systems described in Ref. [21] for the purpose of reaction channel identification. In this case, the 24 element CsI(Tl) wall was mounted downstream from the plunger to identify recoiling Al nuclei from the target. The coincident detection of an Al nucleus scattered from the target in the CsI(Tl) wall and a γ-ray in TIGRESS was used to identify Coulex events. Waveforms from TIGRESS and the CsI(Tl) detectors were recorded on an event-by-event basis by the TIGRESS DAQ and analyzed offline following the procedure defined in Ref. [21]. The interaction of light charged particles in CsI(Tl) detectors is governed by fast and slow scintillation processes [22]. The contribution of each of these processes to the total amplitude of the waveform contains information about the type of particle interacting with the detector and can be used to construct a particle identification (PID) value [21]. A plot of the PID value versus the total signal amplitude is used for the purpose of separating reaction channels. Such a plot for a single CsI(Tl) detector is shown in Fig. 1. Because data were collected in CsI(Tl)-TIGRESS coincidence mode, the β^- decay of elastically scattered radioactive beam implanted in the CsI(Tl) detectors and the coincident γ-ray decay of the daughter nuclei was a significant source of background which has to be resolved using the PID procedure. Gates were set on the Al nucleus coming from the Coulex reaction and γ-ray spectra in coincidence with the detected Al nuclei were analyzed for the lifetime measurement.

III. Data analysis and results. Spectra were recorded at three target-degrader separation distances: 50, 100, and 150 μm; the absolute target-degrader separation distances can be determined from the setup with a precision of <0.5 μm. The analysis procedure follows that of Ref. [23], where RDM line shapes simulated using Geant4 [24,25] are compared to line shapes observed in the experiment. The structure of the Geant4 simulation code is taken from Ref. [26] and implements a single step Coulex reaction via the analytic solutions derived in Ref. [27]. No evidence for the population of higher-lying states in ^{94}Sr was observed in the experiment, and the contributions of unobserved feeding are negligible compared to the statistical uncertainty imposed by the limited statistics in the RDM spectra for the $2_1^+ \rightarrow 0_1^+$ transition of interest. Therefore, multiple-step Coulomb excitations which

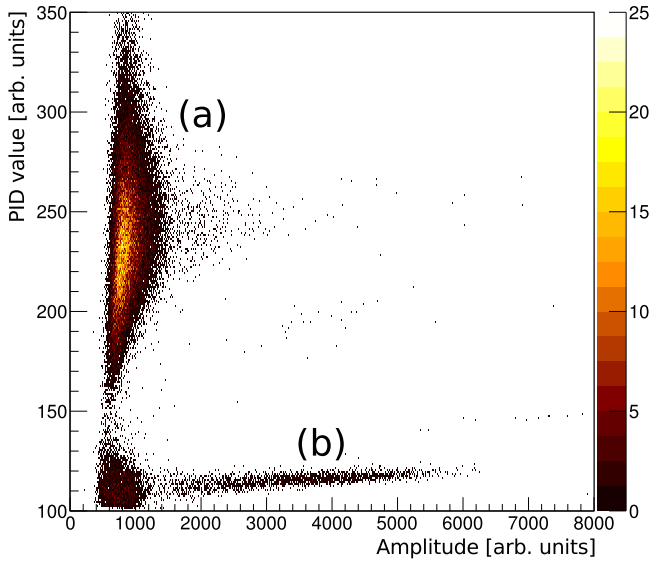

FIG. 1. A particle identification plot for a single CsI(Tl) detector. The PID scheme in the data analysis is performed on a detector-by-detector basis and can distinguish between (a) electrons from the β^- decay of the implanted radioactive beam and (b) Al recoils arising from Coulomb excitation.

populate states that feed the 2_1^+ state were not considered in the reaction model. Since Coulex kinematics give a range of scattering momenta for the projectile, TIGRESS detectors at fixed laboratory angles are sensitive to a range of γ-ray Doppler shifts depending on the kinematics of the reaction. It would be preferable to group the TIGRESS-CsI(Tl) detector pairs by the Doppler shift factor given by Eq. (1),

$$D = \frac{\sqrt{1-\beta_p^2}}{1-\beta_p \boldsymbol{e_p}\cdot\boldsymbol{e_\gamma}}, \tag{1}$$

where β_p is the velocity of the projectile, $\boldsymbol{e_p}$ is the unit vector along the projectile momentum direction, and $\boldsymbol{e_\gamma}$ is the unit vector along the γ-ray emission direction. However, β_p and $\boldsymbol{e_p}$ could not be accurately measured on an event-by-event basis in this experiment and kinematic reconstruction of the reaction is therefore not possible from the measured data. This information can be accessed in Geant4 and was used to divide the TIGRESS-CsI(Tl) detector pairs into kinematic groups based on the Doppler shift of the fast component γ-ray; a summary of the Doppler shift groups used for the analysis is given in Table I.

The determination of the lifetime follows the method of Ref. [28] with one major change. Least-squares based χ^2 statistics (e.g., Neyman's χ^2 or Pearson's χ^2), though typical for this type of analysis, are well known to be inappropriate for low-statistics data. An alternative method which derives a χ^2 statistic from a Poisson maximum likelihood function was used for the analysis of experimental line shapes. A detailed explanation of this method is given in Ref. [29]. The likelihood

TABLE I. TIGRESS/CsI(Tl) detector pair group numbers and their corresponding fast component Doppler shift factors from Eq. (1) for the analysis of RDM γ-ray spectra. The Doppler shift factor is determined by calculating the average Doppler shift in a given detector pair for 10^8 simulated reactions.

Group	Doppler shift factor D	No. of detector pairs
1	$1.025 < D$	306
2	$1.012 < D \leqslant 1.025$	202
3	$0.986 < D \leqslant 1.012$	530
4	$0.975 < D \leqslant 0.986$	188
5	$D \leqslant 0.975$	310

ratio χ^2 of Ref. [29] is defined in Eq. (2),

$$\chi^2 = 2\sum_{i=1}^{k} y_i - n_i + n_i \ln(n_i/y_i), \tag{2}$$

where n_i is the number of counts in the ith bin of the observed line shape and y_i is the number of counts in the ith bin predicted from the model. In this case, the model data are given by Eq. (3),

$$y_i = \alpha_0 s_i + \alpha_1 + \alpha_2 \mathrm{erfc}\left(\frac{i-c}{w\sqrt{2}}\right), \tag{3}$$

where s_i is the Geant4-simulated line shape in the ith bin, erfc is the complementary error function with centroid c and width w, and the α parameters, which are the only free parameters of the model, define the amplitude of the scaling (α_0) and background (α_1, α_2). The α's of Eq. (3) were determined independently for each Doppler shift group and each distance at a fixed input lifetime τ by numerical minimization of Eq. (2).

The total unreduced likelihood ratio χ^2 for the input lifetime is determined by summing over all groups and all target-degrader separation distances; a distribution of the total likelihood ratio χ^2 as a function of input lifetime was

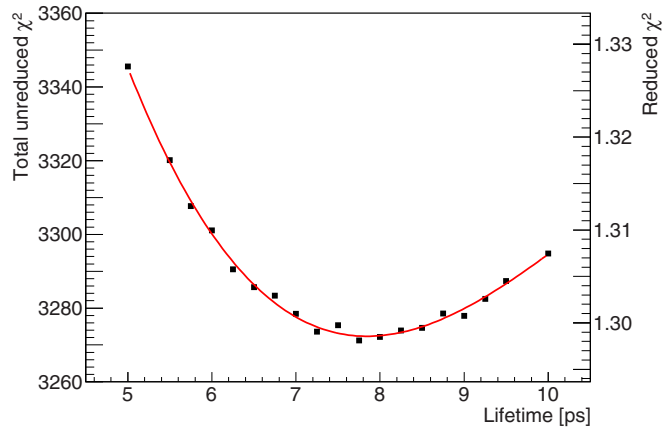

FIG. 2. The distribution of total unreduced χ^2 values as a function of input lifetime (black squares). The corresponding reduced χ^2 value is given on the right axis. The cubic polynomial fit (red line) was used to determine the best fit lifetime and uncertainty.

TABLE II. The measured lifetime and $B(E2;2_1^+ \rightarrow 0_1^+)$ value for the current work compared to the previous fast timing measurement of Ref. [4] with corresponding statistical uncertainties from the χ^2 analysis given at the 1σ level. Discussion of the systematic uncertainties can be found in Sec. III.

Reference	Technique	Lifetime τ (ps)	$B(E2;2_1^+ \rightarrow 0_1^+)$ (e^2b^2)
Current work	Coulex-RDM	$7.80^{+0.50}_{-0.40}$(stat.) $\pm$ 0.07(sys.)	$0.0253^{+0.0014}_{-0.0015}$(stat.) $\pm$ 0.0002(sys.)
Ref. [4]	Fast timing	10 ± 4	0.020 ± 0.008

constructed and is shown in Fig. 2. A best fit lifetime of $\tau_{\text{min.}} = 7.8^{+0.5}_{-0.4}$ ps was determined from the minimum of a cubic polynomial fit of the distribution with the statistical uncertainty given at 1σ extracted from $\chi^2_{\text{min.}} + 1$. The precision of the absolute target-degrader separation distance discussed in Sec. II and the effect on the best fit lifetime as the fit range for the χ^2 determination was varied by $\pm 30\%$ were investigated as possible sources of systematic error. Their impact was assessed independently and added in quadrature to give a final systematic uncertainty of 0.07 ps. The best fit lifetime and corresponding $B(E2;2_1^+ \rightarrow 0_1^+)$ value are compared to previous results from Ref. [4] in Table II. Simulated line shapes for Doppler shift groups 1 and 5 with the best fit lifetime from Table II are shown along with experimental data in Fig. 3.

IV. Discussion. The lifetime of the 2_1^+ state in ^{94}Sr, measured here for the first time using Coulex-RDM with a low-energy radioactive beam, yields a measured $B(E2;2_1^+ \rightarrow 0_1^+)$ value $\sim$25% larger than previously reported in Ref. [4]. This is similar to the larger $B(E2;2_1^+ \rightarrow 0_1^+)$ value relative to that reported by Ref. [4] measured in ^{96}Sr in a recent Coulomb excitation experiment [16]. Despite the larger $B(E2)$ values, both the current result and the result of Ref. [16] are consistent with the results in Refs. [4,10], and the observation of a nearly spherical baseline prior to the rapid onset of deformation at $N = 60$ has been confirmed.

Available experimental data in the Sr isotopes demonstrate a number of similarities to the neighboring Zr isotopes, where a QPT interpretation based on the calculations in Ref. [2] has been applied. Additionally, the presented experiment represents the most precise $B(E2;2_1^+ \rightarrow 0_1^+)$ measurement achieved in this region and demonstrates the power of the Coulex-RDM technique implemented using TIP and TIGRESS for low-energy radioactive beams at TRIUMF.

The onset of deformation in the Sr isotopes has been described by a number of theoretical models. The $B(E2;2_1^+ \rightarrow 0_1^+)$ values from these models, calculated from deformation parameters or intrinsic quadrupole moments

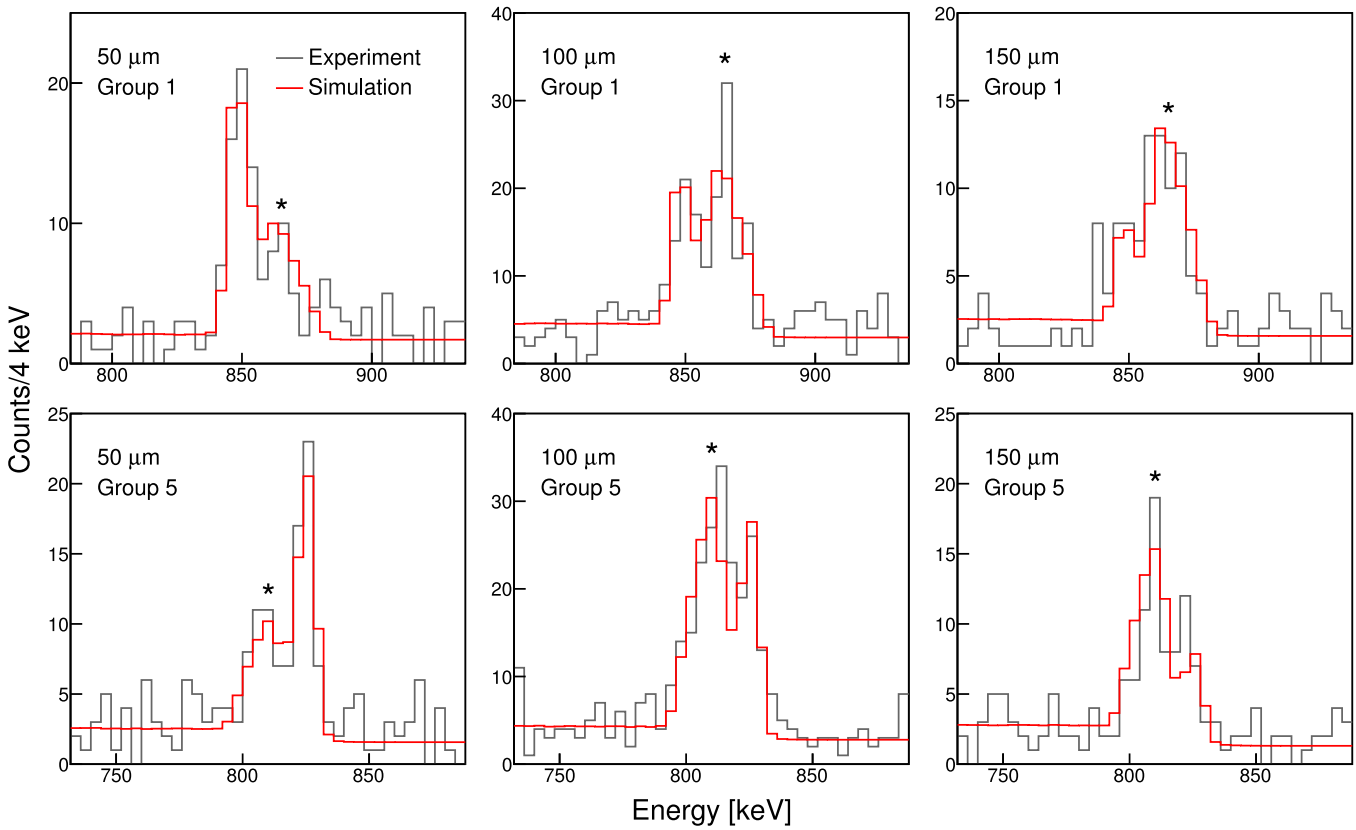

FIG. 3. Experimental data (gray) and the simulated line shape corresponding to the best fit lifetime $\tau_{\text{min.}} = 7.8$ ps (red) for groups 1 and 5; see Table I for details regarding the detector groups. The peak corresponding to the "fast component" decays is labeled with the $*$ symbol.

TABLE III. Theoretical predictions for the $B(E2;2_1^+ \rightarrow 0_1^+)$ value from Refs. [12–15]. Definitions for the abbreviations in the "Technique" column are given in Sec. I. For comparison, see the experimental result presented in Table II.

Reference	Technique	$B(E2)$ (e^2b^2)
Ref. [12]	QPH	0.0006
Ref. [13]	N-S WS	0.017
Ref. [14]	RMF	0.077
Ref. [15](a)	FRDM	0.091
Ref. [15](b)	ETFSI	0.053

when not directly available, are shown in Table III and along with the experimental data in Fig. 4. While the existing models are qualitatively successful, a number of important discrepancies with the data exist. The quadrupole plus pairing Hamiltonian approach of Ref. [12] successfully predicts the increase in $B(E2;2_1^+ \rightarrow 0_1^+)$ at $N = 60$ but systematically underpredicts the $B(E2;2_1^+ \rightarrow 0_1^+)$ strength for the lighter Sr isotopes indicating a larger single-particle character than observed experimentally. The Nilsson-Strutinsky method of Ref. [13], which most accurately reproduces the $B(E2;2_1^+ \rightarrow 0_1^+)$ value for ^{94}Sr, predicts the onset of deformation at $N = 58$ rather than $N = 60$. Models which predict a larger degree of deformation in the lighter Sr isotopes [14,15] both overpredict the collectivity of the $2_1^+ \rightarrow 0_1^+$ transition in ^{94}Sr and fail to reproduce the sharp rise in $B(E2;2_1^+ \rightarrow 0_1^+)$ strength at $N = 60$. It should be noted that while prediction of the onset of deformation in the Sr isotopes remains a challenge, the $B(E2)$ values predicted by the existing models vary by nearly three orders of magnitude for ^{94}Sr, as shown in Table III, indicating that the structure of the lighter Sr isotopes is still not well understood.

Detailed shell model calculations, like those of Ref. [2] which take into account the recent experimental results may help shed light on the specific mechanisms of shell evolution in the Sr isotopes. However, spectroscopic information in this region is still very limited: quadrupole moments, lifetimes, and $B(E2)$ values beyond the 2_1^+ state in both ^{94}Sr and ^{96}Sr remain largely unknown and present a challenge for

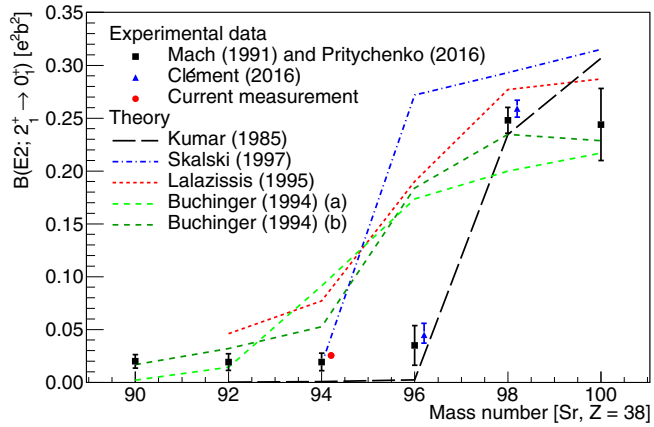

FIG. 4. Systematics of $B(E2;2_1^+ \rightarrow 0_1^+)$ values in the Sr isotopes demonstrating the onset of deformation from $N = 58$ to $N = 60$. The uncertainties in the experimental data are given at 1σ. For the current measurement, the size of the uncertainty is smaller than the data point. Experimental results are Mach (1991) [4], Prytychenko (2016) [10], and Clément (2016) [16]; the theory data are taken from Kumar (1985) [12], Skalski (1997) [13], Lalazissis (1995) [14], and Buchinger (1994) [15].

modern radioactive ion beam facilities. Precise measurements of excited state properties such as lifetimes and $B(E2)$ values in these nuclei can provide important feedback to guide the development of nuclear models which aim to explain the structure of nuclei in this region. The consistency between the data of Refs. [4,10], the recent results for ^{96,98}Sr [16], and the presented measurement demonstrate the need for new theory which can explain the sudden onset of deformation.

The presented measurement establishes the presence of a near-spherical baseline necessary for the possible QPT interpretation of the onset of deformation in the Sr isotopes. Additionally, a new device for RDM measurements at TRIUMF has been commissioned. Techniques for the application of the RDM with TIP for low-intensity radioactive beams and analysis methods using Geant4-simulated line shapes have been developed, opening up many opportunities for precision lifetime measurements at TRIUMF.

[1] T. Otsuka and Y. Tsunoda, J. Phys. G: Nucl. Part. Phys. **43**, 024009 (2016).
[2] T. Togashi, Y. Tsunoda, T. Otsuka, and N. Shimizu, Phys. Rev. Lett. **117**, 172502 (2016).
[3] C. Kremer *et al.*, Phys. Rev. Lett. **117**, 172503 (2016).
[4] H. Mach, F. K. Wohn, G. Molnr, K. Sistemich, J. C. Hill, M. Moszyski, R. Gill, W. Krips, and D. S. Brenner, Nucl. Phys. A **523**, 197 (1991).
[5] H. Mach, M. Moszynski, R. L. Gill, F. K. Wohn, J. A. Winger, J. C. Hill, G. Molnr, and K. Sistemich, Phys. Lett. B **230**, 21 (1989).
[6] H. Ohm, G. Lhersonneau, K. Sistemich, B. Pfeiffer, and K.-L. Kratz, Z. Phys. A: At. Nucl. **327**, 483 (1987).
[7] G. Lhersonneau, H. Gabelmann, N. Kaffrell, K.-L. Kratz, B. Pfeiffer, and K. Heyde, Z. Phys. A: At. Nucl. **337**, 143 (1990).
[8] L. Grodzins, Phys. Lett. **2**, 88 (1962).
[9] S. Raman, C. W. Nestor, and P. Tikkanen, At. Data Nucl. Data Tables **78**, 1 (2001).
[10] B. Prytychenko, M. Birch, B. Singh, and M. Horoi, At. Data Nucl. Data Tables **107**, 1 (2016).
[11] Nudat 2.6, http://www.nndc.bnl.gov/nudat2.
[12] A. Kumar and M. R. Gunye, Phys. Rev. C **32**, 2116 (1985).
[13] J. Skalski, S. Mizutori, and W. Nazarewicz, Nucl. Phys. A **617**, 282 (1997).
[14] G. Lalazissis and M. Sharma, Nucl. Phys. A **586**, 201 (1995).
[15] F. Buchinger, J. E. Crawford, A. K. Dutta, J. M. Pearson, and F. Tondeur, Phys. Rev. C **49**, 1402 (1994).
[16] E. Clément *et al.*, Phys. Rev. Lett. **116**, 022701 (2016).
[17] A. Dewald, O. Möller, and P. Petkov, Prog. Part. Nucl. Phys. **67**, 786 (2012).

[18] A. Görgen and W. Korten, J. Phys. G: Nucl. Part. Phys. **43**, 024002 (2016).
[19] R. E. Laxdal, Nucl. Instrum. Methods Phys. Res., Sect. B **204**, 400 (2003).
[20] C. E. Svensson *et al.*, J. Phys. G: Nucl. Part. Phys. **31**, S1663 (2005).
[21] P. Voss *et al.*, Nucl. Instrum. Methods Phys. Res., Sect. A **746**, 87 (2014).
[22] M. Bendel, R. Gernhuser, W. F. Henning, R. Krücken, T. L. Bleis, and M. Winkel, Eur. Phys. J. A **49**, 69 (2013).
[23] K. Starosta *et al.*, Phys. Rev. Lett. **99**, 042503 (2007).
[24] S. Agostinelli *et al.*, Nucl. Instrum. Methods Phys. Res., Sect. A **506**, 250 (2003).
[25] J. Allison *et al.*, IEEE Trans. Nucl. Sci. **53**, 270 (2006).
[26] P. Adrich, D. Enderich, D. Miller, V. Moeller, R. P. Norris, K. Starosta, C. Vaman, P. Voss, and A. Dewald, Nucl. Instrum. Methods Phys. Res., Sect. A **598**, 454 (2009).
[27] K. Alder, A. Bohr, T. Huus, B. Mottelson, and A. Winther, Rev. Mod. Phys. **28**, 432 (1956).
[28] P. Voss, T. Baumann, D. Bazin, A. Dewald, H. Iwasaki, D. Miller, A. Ratkiewicz, A. Spyrou, K. Starosta, M. Thoennessen, C. Vaman, and J. A. Tostevin, Phys. Rev. C **90**, 014301 (2014).
[29] S. Baker and R. D. Cousins, Nucl. Instrum. Methods Phys. Res. **221**, 437 (1984).